The Closed State of a H^+ Channel Helical Bundle Combining Precise Orientational and Distance Restraints from Solid State NMR†

Katsuyuki Nishimura,[‡,§,||] Sanguk Kim,[‡,||,⊥] Li Zhang,[‡,#,£] and T. A. Cross*[,§,⊥,#]

National High Magnetic Field Laboratory, Department of Chemistry & Biochemistry, and Institute of Molecular Biophysics, Florida State University, Tallahassee, Florida 32310

Received June 11, 2002; Revised Manuscript Received August 5, 2002

ABSTRACT: An interhelical distance has been precisely measured by REDOR solid-state NMR spectroscopy in the transmembrane tetrameric bundle of M2-TMP, from the M2 proton channel of the influenza A viral coat. The high-resolution structure of the helical backbone has been determined using orientational restraints from uniformly aligned peptide preparations in hydrated dimyristoylphosphatidylcholine bilayers. Here, the distance between $^{15}N_{\pi}$ labeled His37 and $^{13}C_{\gamma}$ labeled Trp41 is determined to be less than 3.9 Å. Such a short distance, in combination with the known tilt and rotational orientation of the individual helices, permits not only a determination of which specific side chain pairings give rise to the interaction, but also the side chain torsion angles and restraints for the tetrameric bundle can also be characterized. The resulting proton channel structure is validated in a variety of ways. Both histidine and tryptophan side chains are oriented in toward the pore where they can play a significant functional role. The channel appears to be closed by the proximity of the four indoles consistent with electrophysiology and mutagenesis studies of the intact protein at pH 7.0 and above. The pore maintains its integrity to the N terminal side of the membrane, and at the same time, a cavity is generated that appears adequate for binding amantadine. Finally, the observation of a 2 kHz coupling in the PISEMA spectrum of $^{15}N_{\pi}$His37 validates the orientation of the His37 side chain based on the observed REDOR distance.

Channel gating is induced by a variety of environmental changes, and it is functionally achieved by a diversity of mechanisms. The M2 proton channel of influenza A virus is pH activated. Under neutral and basic conditions this channel is closed (*1*, *2*). On the basis of mutagenesis studies, an interaction between His37 and Trp41 has been suggested as the mechanism for sterically closing this channel (*3*). Here, using solid-state NMR spectroscopy of the transmembrane peptide from M2 protein in hydrated lipid bilayers, this mechanism is investigated.

The M2 proton channel is essential for influenza infection. This tetrameric channel (*4*) permits the uncoating of the viral RNA and fusion of the viral membrane with the endosomal wall (*5*). Blockage of this channel with amantadine prevents fusion of these membranes (*6*). M2 protein is a 97 residue protein with a single transmembrane domain (residues 25−43) between N and C hydrophilic terminal domains (*5*, *7*, *8*). A 25 residue polypeptide (M2-TMP) that spans the hydrophobic membrane region and has a few hydrophilic residues on either end (residues 22−46) also shows evidence for amantadine binding (*9*) and proton conductance (*1*), although Tobler and co-workers (*10*) using truncated M2 protein have questioned these latter results. Despite this, M2-TMP is still viewed as an excellent model system for studying the proton channel formed by a tetramer of M2 protein. Evidence has been presented that this peptide is oligomeric in bilayers (*11*) and tetrameric in micelles (*12*). Furthermore, a high-resolution characterization of the polypeptide backbone has been achieved (*13*), including a precise determination of the helical tilt and rotational orientation relative to the anisotropic membrane environment. The identity of the residues lining the pore has been known for years (*14*, *15*), and in combination with the rotational orientation of the helices, it is now recognized that the tetrameric bundle must be left-handed. This positions the few hydrophilic residues of the transmembrane region oriented toward the aqueous pore (*16*). Moreover, the observation of single resonances from single site labels suggests that the tetramer is symmetric or at least pseudosymmetric (*13*). Numerous models of this tetrameric bundle have been published (*15*, *17*−*21*).

There are numerous advantages in using orientational restraints derived from solid-state NMR to develop 3D structures (*22*, *23*). Each orientational observation restrains

† This work was supported by the National Science Foundation, MCB99-86036 and the National Institutes of Health, AI23007. The work was performed largely at the National High Magnetic Field Laboratory, supported by Cooperative Agreement (DMR-0084173) and the State of Florida.

* To whom correspondence should be addressed. E-mail: cross@magnet.fsu.edu. Tel: 850-644-0917. Fax: 850-644-1366.

‡ National High Magnetic Field Laboratory.

§ Present address: Yokohama National University, 79−5 Tokiwadai, Hodogaya-ku,Yokohama,Kanagawa, 240-8501, Japan.

Department of Chemistry & Biochemistry.

|| These authors contributed equally to the work.

⊥ Institute of Molecular Biophysics.

£ Present address: Amgen Inc. One Amgen Center Drive, MS 18S-1-A, Thousand Oaks, CA 91320.

[1] Abbreviations: DMPC, dimyristoylphosphatidylcholine; TFE, trifluoroethanol; NMR, nuclear magnetic resonance; REDOR, rotational echo double resonance; PISEMA, polarization inversion spin exchange at the magic angle; CPMAS, cross polarization magic angle spinning.

10.1021/bi0262799 CCC: $22.00
Published on Web 10/12/2002

the macromolecular structure to the laboratory frame of reference and to the lipid bilayer frame of reference in membrane protein samples. The assembly of a structure from such restraints does not result in the summation of errors, because each restraint is interpreted independently. One of the most important advantages for these restraints is that α-helical structures are imaged directly in the PISEMA (*24*) spectra that correlates anisotropic $^{15}N-^{1}H$ dipolar and ^{15}N chemical shift interactions (*25*, *26*). Indeed, the tilt of a transmembrane helix can be determined without resonance assignments and the rotational orientation without complete resonance assignments. This fixes the orientation of the protein relative to its environment, an essential feature of membrane protein structural characterization. While, these orientational restraints are very precise structural restraints, they are not able to position domains or potentially even secondary structural elements relative to each other. Here, we use a distance restraint also derived from solid-state NMR using a sample of hydrated lipid bilayers to initiate a quaternary structural characterization of this proton channel.

Solid-state NMR distance restraints have a considerable history in structural elucidation of oligopeptides (*27*−*30*). Furthermore, solid-state NMR distance restraints have been used to characterize local structural details in macromolecular complexes (*31*−*35*), including helix-helix interactions in a membrane environment (*36*−*39*). Here structural conclusions about the closed state of the M2-TMP tetramer are achieved from a REDOR (rotational echo double resonance) (*40*) distance characterization between His37 and Trp41 in hydrated bilayer preparations of this peptide. Previously, such a distance measurement and analysis has been successfully demonstrated in a liquid crystalline lipid preparation of gramicidin A (*41*).

EXPERIMENTAL PROCEDURES

Sample Preparation. Isotopically labeled amino acids (99% enriched) [$^{13}C_\gamma$]Trp and [$^{15}N_\pi$]His were purchased from Cambridge Isotope Laboratories (Cambridge, MA). Fmoc N-hydroxysuccinimide ester was purchased from SIGMA Chemical Company (St. Louis, MO). Isotopically labeled Fmoc−[$^{13}C_\gamma$]Trp was chemically synthesized based on Paquet's method (*42*) with a slight modification to avoid oxidization of the side chain. In the final step of this synthesis, the reacted Fmoc−Trp was precipitated by slowly adding HCl to an 8.6 mM 2-mercaptoethanol, 20 mM Fmoc−Trp, pH 9.0 solution until the pH was lowered to 2.0 at 4 °C. After precipitation, Fmoc−Trp was filtered out and washed with cold H_2O twice and lyophilized overnight. The obtained Fmoc−Trp was recrystalized from dichloromethane/hexane. Similarly, Fmoc [$^{15}N_\pi$] His was chemically synthesized (*43*).

The ^{13}C- and ^{15}N-doubly labeled M2-TMP (NH_2-Ser_{22}-Ser_{23}-Asp_{24}-Pro_{25}-Leu_{26}-Val_{27}-Val_{28}-Ala_{29}-Ala_{30}-Ser_{31}-Ile_{32}-Ile_{33}-Gly_{34}-Ile_{35}-Leu_{36}-[$^{15}N_\pi$]His_{37}-Leu_{38}-Ile_{39}-Leu_{40}-[$^{13}C_\gamma$]-Trp_{41}-Ile_{42}-Leu_{43}-Asp_{44}-Arg_{45}-Leu_{46}-CO_2H) was synthesized on the basis of solid-phase methods using an Applied Biosystems-Model 433A peptide synthesizer (*16*). The cleavage procedure was optimized based on a standard TFA protocol that minimizes side reactions. The purity of the cleaved peptide was assessed by MASS spectroscopy and reverse phase HPLC to be 95%.

To prepare an unoriented hydrated lipid bilayer sample, M2-TMP and dimyristoylphosphatidylcholine (DMPC) in a 1:16 molar ratio were cosolubilized in trifluoroethanol (TFE). After lyophilization, the white powder was hydrated by adding 50% (by total sample dry weight) pH 7.0, HPLC-grade water, followed by incubation for 2 days at 42 °C. The sample was then dispersed in 30 mL of 20 mM citric/Na_2HPO_4 buffer at pH 7.0 and incubated at 45 °C for 2 h before centrifuging at 20 000*g* for 3 h. The supernatant was used to check the pH of the samples. After excess water was removed, the pellet was transferred to an eppendorf tube, tightly sealed to maintain the same hydration level, and then incubated at 45 °C for 2 days. Finally, the sample was transferred to a glass insert for a Bruker 7 mm spinner (Wilmad, Buena, NJ) and sealed with epoxy to maintain the hydration level of the sample and to keep the sample within a homogeneous volume of the RF field (i.e., within 90% of the maximum value of the RF field) (*44*). Signals arising from epoxy were subtracted from the solid-state NMR spectra.

To prepare an oriented bilayer sample, 20 mg of M2-TMP and 38.5 mg of DMPC (1:8 molar ratio) were codissolved in 1.5 mL of TFE. The sample was spread on 50 glass slides having dimensions of $5.8 \times 15 \times 0.07$ mm^3. After drying the organic solvent from the slides, approximately 1.2 μL of buffer (0.2 M phosphate and 0.1 M citric acid, pH 7.0) was added to each slide, and then they were stacked into a glass tubing with a 6.0×6.0 mm^2 internal dimension cross section. The square tubing was sealed and the sample was incubated for two weeks at 45 °C prior to recording spectroscopic data.

Solid-State NMR. The magic angle spinning NMR experiments were recorded on a Bruker DMX-300 NMR spectrometer equipped with a Bruker CPMAS triple resonance probe for 7 mm o.d. spinners. The ^{1}H, ^{13}C, and ^{15}N resonance frequencies were 300.16, 75.64, and 30.55 MHz, respectively. The π pulse lengths for ^{13}C and ^{15}N nuclei were 10.8 and 11.8 μs, respectively. Cross-polarization with a contact time of 1 ms, ^{1}H decoupling with a field of 75 kHz, and a recycle delay of 4s were used.

The heteronuclear distance was obtained by means of solid-state NMR REDOR experiments (*40*). ^{13}C-REDOR was performed on a DMX-300 with an XY8-pulse sequence (*45*) for irradiation of ^{15}N nuclei to compensate for errors in the flip angle, off resonance effect, and variation in the H_1 field (*44*). The spinning speed was controlled at 4000 ±1 Hz, and the experiments were performed at 38 °C. REDOR and full echo spectra were recorded at various dipolar evolution times, $N_c\tau_r$, (where N_c and τ_r are the rotor cycle number and rotor period, respectively) from 2 to 16 ms to observe reasonable dipolar dephasing of the signals. The normalized REDOR difference (REDOR factor) was defined as S_f/S_0 (= REDOR/full echo) to cancel the decay of the signal intensities due to the transverse relaxation process. The number of acquisitions ranged from 6000 to 34 400 to achieve reasonable signal-to-noise ratios. The contribution of dipolar dephasing from neighboring natural abundant ^{15}N nuclei has been neglected because ^{15}N is such a rare nucleus in proteins (*46*). The best-fit theoretical curve was calculated by varying the heteronuclear dipolar coupling constants $D = -(\mu_0/4\pi)^*(\gamma_I\gamma_S h/2\pi r^3)$.

^{15}N NMR spectroscopy of the aligned sample was obtained on a home-built 400 MHz (40.6 MHz for ^{15}N) spectrometer using an 89 mm bore Oxford magnet and a Chemagnetics data acquisition system. A home-built double resonance probe was used with a square solenoid coil. Conditions for the PISEMA experiment are as described previously (*47*). All ^{15}N chemical shifts are defined relative to a saturated solution of $^{15}NH_4NO_3$ at 0 ppm.

Computational Methods. Initial symmetric, tetrameric bundle structures were constructed by duplication of the structurally refined helix and rotating them about the *z*-axis by 90°, 180°, and 270°, respectively. Then helices were translated in the *x*,*y* plane by an initial helical axis separation of 11 Å. The parameters for the tetramer helical bundle include helix tilt angle, rotational angle about the helix axis, helix crossing point and helical separation distance (*48*, *49*). The helical tilt angle and rotational angle are already characterized by numerous orientational restraints from 2D PISEMA data (*13*). But the helical crossing point and helical separation distance are not defined by orientational restraints. Previous studies from diverse helical bundles (*50*) have reported a narrow range for these parameters, including a range from 10 to 11 Å for the helical axis separation and a crossing point close to the middle of the helix. These parameters have routinely been used in helical bundle models (*15*, *19*, *49*). Here the helical separation distance in M2-TMP was searched using translations of the helices in the *x*,*y* plane from initial coordinates in decrements of 0.2 Å until the helix-helix contacts were optimized.

To maintain the integrity of the pore, the helical crossing point must be located near the middle of the transmembrane helix. Only in this way is the pore surrounded by the protein along its entire length. Moreover, in the transmembrane helix of M2, the Gly34 residue is located in the middle of the helix, suggesting that the location of the helix−helix closest approach is at this site where the absence of a side chain facilitates close approach (*36*, *51*).

The resulting tetrameric bundle structure was used to search the side chain orientations in accord with the experimentally measured distance between $^{15}N_{\pi}$His37 and $^{13}C_{\gamma}$Trp41. The rotamer states of His and Trp side chains and their nomenclature are adopted from the "penultimate rotamer library" (*52*). Both χ_1 and χ_2 angles of the residues were searched extensively using 10° increments to discern whether the interaction was intramolecular or intermolecular and to find out which residues accounted for the observed spin interaction before characterizing the rotameric states of the side chains. Each of the structures were energy minimized using steepest descent and conjugate gradient energy minimization protocols with CHARMM (*53*). The distances of each rotameric pair were examined before and after the energy minimization to check the distance and their van der Waals clash.

RESULTS AND DISCUSSION

Figure 1 shows high sensitivity signals obtained from magic-angle spinning samples of M2-TMP in DMPC lipid bilayers above the gel to liquid crystalline phase transition temperature. All experiments in this study were performed on samples at pH 7.0 in the essentially closed state of the proton channel. Resonances from $^{15}N_{\pi}$His37 and $^{13}C_{\gamma}$Trp41 are both quite broad suggesting significant slow motions that induce efficient T_2 relaxation.

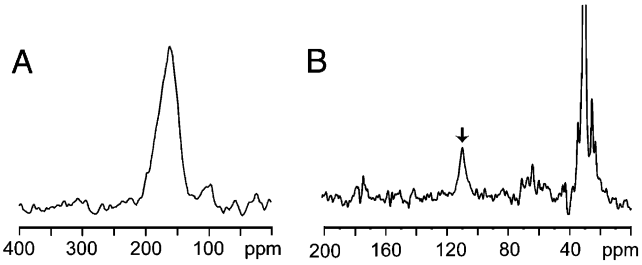

FIGURE 1: ^{1}H decoupled ^{15}N and ^{13}C CPMAS spectra of a 10 mg sample of [$^{15}N_{\pi}$] His37−[$^{13}C_{\gamma}$] Trp41 doubly labeled M2-TMP in hydrated (50% by wt.) DMPC lipid bilayers observed at a 4 kHz spinning rate with 1 ms mixing time and a 4 s recycle delay, 38 °C and pH 7.0. (A) ^{15}N spectrum; the small signal around 100 ppm is due to backbone amide natural abundant signals. (B) ^{13}C spectrum shows considerable natural abundant signals in addition to the labeled C_{γ} signal at 109 ppm (indicated by arrow). The spectrum is a difference spectrum involving the subtraction of the epoxy signals obtained in a separate spectrum. This causes a minor distortion in the aliphatic lipid signals.

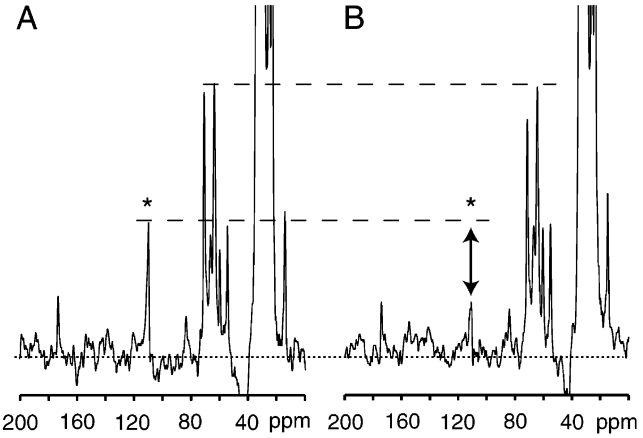

FIGURE 2: ^{13}C-observed rotor-synchronized spin−echo experiments of a 10 mg sample of [$^{15}N_{\pi}$] His37−[$^{13}C_{\gamma}$] Trp41 labeled M2-TMP using an $N_c\tau_r$ value of 12 ms. The 16 000 transients were acquired at 4000 ± 1 Hz spinning rate control. As in Figure 1, the epoxy signals are subtracted. (A) ^{13}C-observed full-echo spectrum. (B) ^{13}C-observed REDOR spectrum (^{15}N dipolar dephased). The upper dotted lines indicate reference signals from lipid (nondephasing), which are compared to lower dotted lines for observed $^{13}C_{\gamma}$ signals marked by ∗ (dipolar dephased at REDOR).

Figure 2 shows an example of the ^{13}C observed REDOR spectra and full echo spectrum for intensity comparison. Efficient dephasing is observed in this REDOR spectrum at 12 ms (48 rotor cycles at 4 kHz). Such dipolar dephasing suggests close proximity of the histidine and tryptophan side chains in the M2-TMP tetrameric structure. In Figure 3 the dipolar dephasing is shown by plotting the normalized REDOR intensity of the $^{13}C_{\gamma}$Trp41 site dephased by $^{15}N_{\pi}$His37 divided by the full echo intensity versus $N_c\tau_r$. The result is a 63 Hz coupling with a generous error bar of ±12 Hz based on the signal-to-noise ratio in the spectra. 51 Hz equates to a maximum distance of 3.9 Å for this REDOR data, while 75 Hz is consistent with a 3.4 Å distance, assuming no motional averaging of the dipolar interaction. It has previously been reported that the M2-TMP structure rotates about the bilayer normal at a rate that is fast compared to the ^{15}N chemical shift anisotropy of the backbone amide sites (*47*).

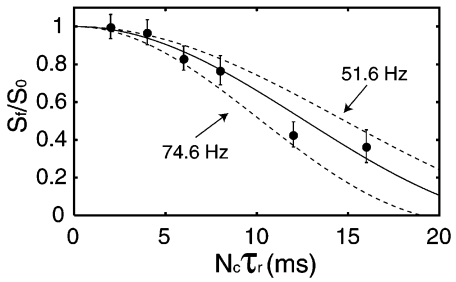

FIGURE 3: Normalized REDOR intensity for [$^{15}N_\pi$] His37−[$^{13}C_\gamma$] Trp41 doubly labeled M2-TMP as a function of $N_c\tau_r$ with best-fit theoretical curves. Error bars are calculated according to the S/N ratio of spectra. Determined dipolar coupling constant was 63 ± 12 Hz. These data show the efficient dipolar dephasing of the $^{13}C_\gamma$ site.

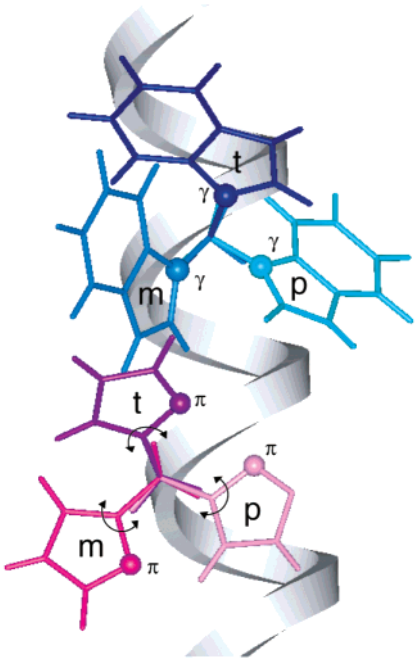

FIGURE 4: His37 and Trp41 search of χ_1 conformational space for a short distance between N_πHis37 and C_γTrp41. The p (g+), t, and m (g−) rotameric states are labeled. Both p rotameric states generate considerable steric clash with the high-resolution structure of the α-helical backbone. Note that while the distance is also dependent on the His χ_2 torsion angle, it is not dependent on the Trp χ_2 torsion angle.

Consequently, dipolar interactions such as this one between $^{15}N_\pi$His37 and $^{13}C_\gamma$Trp41 will be motionally averaged by an amount that is dependent upon the angle of this dipolar interaction relative to the motional axis. Hence, the distance determined here from this dipolar interaction is a maximum distance since the coupling is likely to be motionally averaged and therefore the static value would be greater indicating a shorter distance. For much of the following search of conformational space, we will consider the maximum distance of 3.9 Å consistent with the data.

To interpret this distance, the first challenge is to determine which pairs of residues in the symmetric or pseudosymmetric bundle give rise to this strong dipolar interaction. Initially, the possible intramolecular interaction will be considered. While the side chain conformations in this structure are not known, the backbone conformation is well defined in a high precision structure (*13*). In Figure 4 the χ_1 rotameric states for both His37 and Trp41 are illustrated on the experimentally defined α-helical backbone structure. These χ_1 angles for histidine and tryptophan were taken from the recent rotamer library (−65°, **m**inus state; 63°, **p**lus state; −177°, **t**rans state) (*52*). While coordinates of the $^{13}C_\gamma$ site are only dependent on the χ_1 angle, the position of the $^{15}N_\pi$ site is dependent on both χ_1 and χ_2. However, both χ_2 angles were searched to avoid steric clash while a short distance between these two sites was sought.

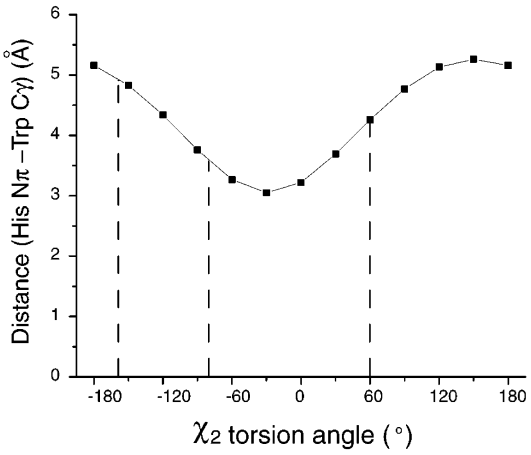

FIGURE 5: With Trp41 in the m χ_1 rotameric state and His37 in the t rotameric state, the N_π−C_γ distance is calculated as a function of His χ_2 angle.

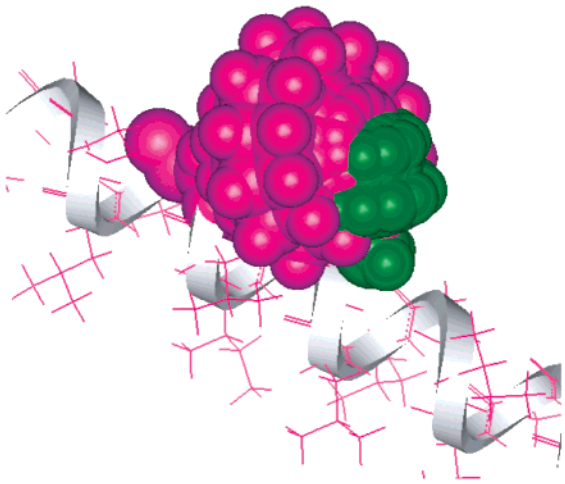

FIGURE 6: With Trp41 in the m χ_1 rotameric state and His37 in the t χ_1 rotameric state, the space filling model of these two side chains (Trp in red; His is green) is presented as a function of χ_2 angles. Models are generated every 30° in χ_2 showing the severe clash between all possible combinations of His and Trp χ_2 angles. Consequently, the only χ_1 states that can generate a short distance between these two residues are not possible because of steric clash.

To avoid steric clash with the main chain helix, neither His37 nor Trp41 can be in the p state (His p state has 0% occurrence and Trp p state has only 3% occurrence) (*52*). In addition, the p state for both His37 and Trp41 are far from all Trp41 and His 37 conformations, respectively. Likewise, the Trp41 t state and His37 m state are not viable options. Therefore, the only possible χ_1 rotameric states are the Trp41 m state and the His37 t state. Using these χ_1 rotameric states, the internuclear distance is plotted in Figure 5 as a function of His37 χ_2. Potential solutions are observed; however, the space filling model for these side chains shown in Figure 6 illustrates severe side chain van der Waals overlap for all possible χ_2 angles.

To further examine the possibility of noncanonical rotameric side chain combinations that could result in the observed dipole coupling, energy minimization calculations were performed. To remove the steric clash described above while maintaining reasonable stereochemistry, the relative weighting of bond lengths and angle potential terms were set larger than the weighting for the nonbonding terms. The ensemble of structures having the range of χ_2 angles for both side chains were energy minimized and the steric clash removed. However, the closest approach was a 5.2 Å interatomic distance at an angle of 66.8°, resulting in a predicted dipolar interaction of less than 5.6 Hz (less than one tenth of the observed interaction), thereby eliminating the possibility that the observed dipolar coupling derives from an intramolecular interaction. Consequently the interaction must arise between side chains of adjacent helices.

Not only is the monomer backbone structure well defined, but the tilt of the helix and its rotational orientation about the helical axis in the lipid bilayer frame of reference are well-known (*13*). To place the hydrophilic side chains toward the pore, the tetrameric bundle must be a left-handed bundle (*16*). Moreover, symmetry or pseudosymmetry for the bundle is assured since single site labels give rise to single resonances (*11*, *13*, *16*, *47*). However, there are two parameters not yet defined for the tetramer, the interhelical separation, defining the helix−helix packing interactions, and the helix−helix crossing point, characterized by a distance along the helical axis. There is little flexibility in the values of either variable, if the integrity of the pore is to be maintained across the membrane. In addition, the separation of the helices must generate a significant van der Waals packing interaction to maintain structural stability of the tetramer. Furthermore, the crossing point must be close to the helical midpoint to avoid flaring of the helices at either end such that the pore integrity is lost. Consequently, these values have not varied greatly among the various published models of the M2-TMP tetramer (*15*, *19*), and they are usually used as a constant during homooligomeric helical bundle modeling (*48*, *49*).

Possible χ_1 rotameric states for His37 and Trp41 are shown in Figure 7. Again, the p state of both side chains are not considered based on steric clash with the backbone. It is clear from the model that the only pairing that represents a close proximity is the Trp41 residue of helix i with the His37 residue of helix i+1. Moreover, the rotameric states that permit close proximity of these two side chains are the t states for both residues. This conformation for histidine generates the important feature that the side chain is turned in toward the pore. For tryptophan it also brings the side chain toward the pore and, in fact, seals the pore, thereby generating the apparent closed state.

Figure 8 shows the calculated internuclear distance and angle to the bilayer normal as a function of His χ_2 angles and for both the m and t χ_1 states. These calculations are also presented for a tenable range of d values from 11.0 to 10.2 Å between helical axes. This is equivalent to 8.0−7.2 Å for the separation of Gly34 C_α carbons. The result from this figure reemphasizes that the His χ_1 rotameric state must be trans, consistent with the previous modeling efforts which have all described the His37 side chain in the trans state. The m state of His37 even at a d value of 10.2 Å results in an internuclear distance of 5 Å or more and an angle for the

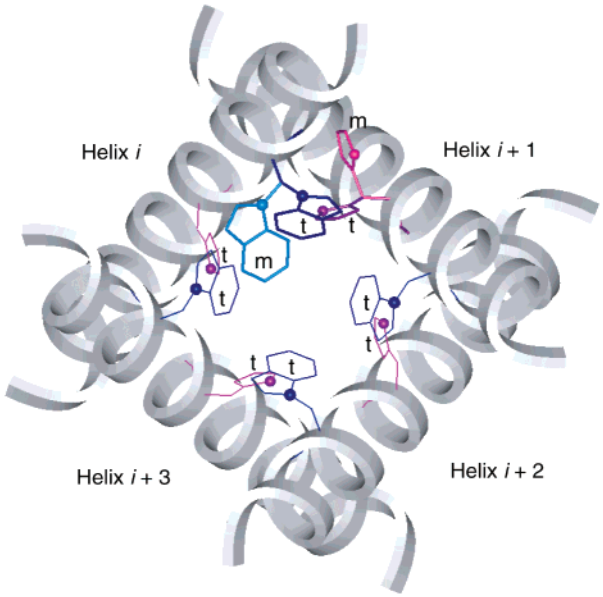

FIGURE 7: For an intermolecular interaction in this tetrameric structure, Trp41 of helix i must be interacting with His37 of helix i+1, and it is readily seen that both χ_1 rotamers must be in the t state. Both t and m states of Trp41 are only shown in helix i, and t states of Trp41 are shown in other helices. Both t and m states of His37 are only shown in helix i+1, and t states of His37 are shown in other helices. The tetramer model structure of M2-TMP was built by the experimentally defined helical tilt and rotational orientation (*12*), the helical axis separation of 10.2 Å, and the crossing point in the middle of the M2-TMP helix.

internuclear vector such that the dipolar interaction is never greater than 15 Hz compared to the observed value of 63 ± 12 Hz.

Upon examining more closely (Figure 9), the orientation of the internuclear vector as a function of the His37 χ_2 angle and the resultant motionally averaged dipolar interaction the χ_2 angle of 172° ±12° is favorable, resulting in a dipolar interaction that is within the observed error bar and within the common-rotamer range of χ_2 angles for histidine (*52*). For Trp41, recall that the internuclear distance is independent of the χ_2 angle, but there are two possible χ_2 rotameric states with angles of −105° and +90°. The +90° conformation results in severe steric clash, and consequently, the Trp41 χ_2 rotameric state is approximately −105°. Therefore, the rotameric states for both side chains for this closed state of the M2-TMP tetramer are defined.

This closed state is shown in Figure 10 with the optimized orientation of His37 ($\chi_1 = -177$; $\chi_2 = +172$) and Trp41 ($\chi_1 = -177$; $\chi_2 = -105$) residues, an interhelical distance, $d = 10.2$ Å, and a helix−helix crossing point in the middle of the helix. While this model illustrates a substantial pore from the N-terminal side, the indole rings block the pore on the C-terminal side. This role for tryptophan has recently been suggested by mutagenesis studies (*3*). The apparent close proximity of the indole and imidazole rings suggests that the REDOR dipolar dephasing could be the result of a $I-S_4$ multispin interaction. However, a deviation from a two-spin approximation in REDOR dephasing is only observable when the third spin contributes more than 12% to the dipolar interaction as reported previously (*54*). Throughout this characterization it has been very difficult to obtain a structural geometry for the His_π and Trp_γ sites that allow for an effective $^{13}C-\ ^{15}N_4$ multispin system in this symmetric or

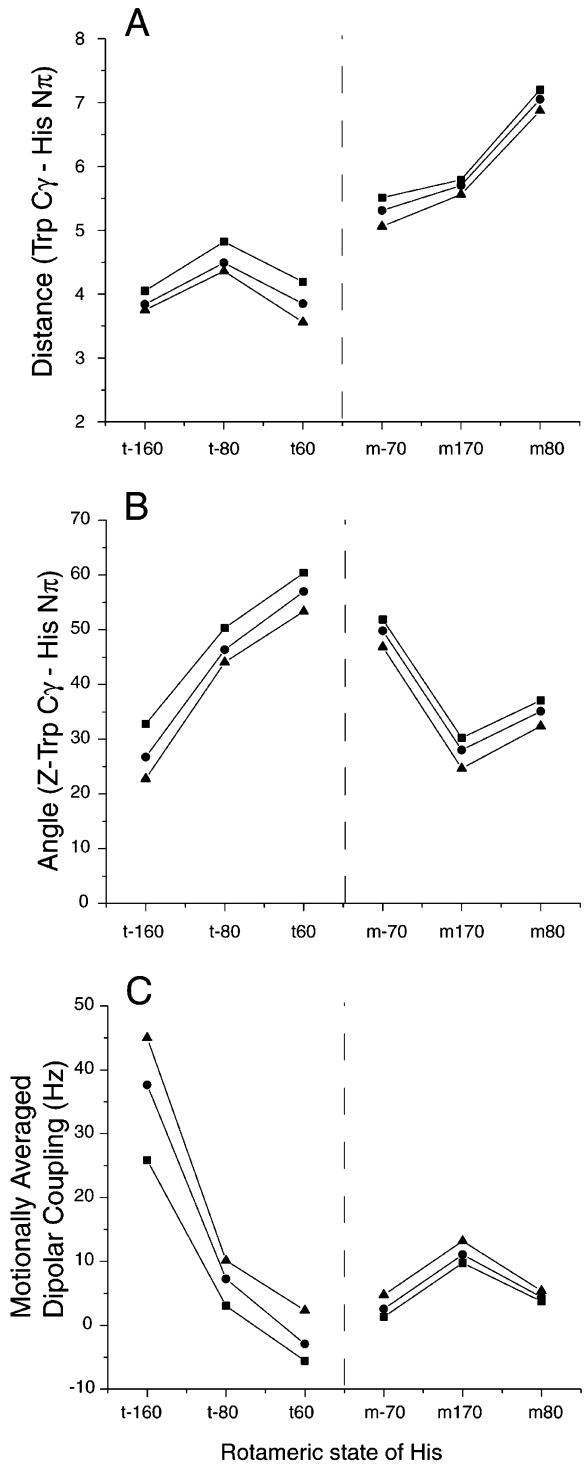

FIGURE 8: Calculation of the motionally averaged dipolar coupling between His N_π and Trp C_γ as a function of the His side chain torsion angles and the interhelical separation, *d* (▲ is 10.2 Å, ● is 10.6 Å, and ■ is 11.0 Å). (A) Much shorter distances are observed for the His χ_1 angle in the **t**rans rather that the **m**inus state. (B) The orientation of the ^{15}N-^{13}C dipolar vector is most favorable for generating a very significant motionally averaged dipolar coupling (C) when χ_1 is trans and χ_2 equals −160°.

pseudosymmetric bundle. Here in this model, the distance to the four $^{15}N_\pi$ sites using the χ_2 value of +172° is 6.99 Å (helix *i* to helix *i*), 3.75 Å (*i* to *i*+1), 8.47 Å (*i* to *i*+2), and 10.25 Å (*i* to *i*+3). Consequently, no significant deviation will be observed by considering more than a two spin approximation (*54*) for the final Trp and His geometry in

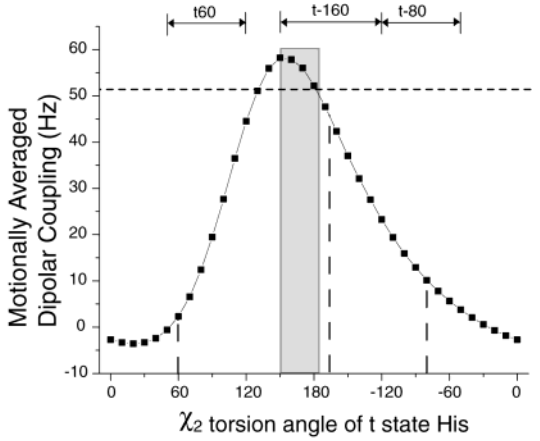

FIGURE 9: Calculation as shown in Figure 8C is refined here as a function of the χ_2 torsion angle. The minimum dipolar coupling from the REDOR measurement is drawn as a dashed line at 51 Hz. Furthermore, the solution set for χ_2 that yields a dipolar coupling greater than 51 Hz and is within the standard range of the χ_2 rotameric state is shaded gray. Note that the other χ_2 rotameric states do not yield viable solutions.

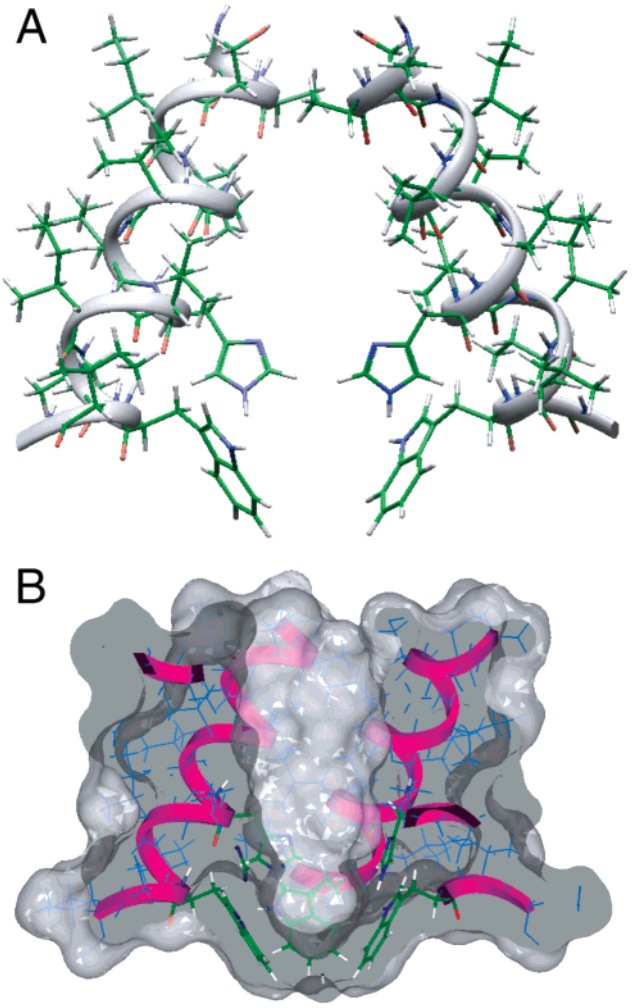

FIGURE 10: Models of M2-TMP based on data obtained at pH 7 when the channel is in its closed state. (A) Two of the four helices are shown illustrating the orientation of the His and Trp side chains. (B) The surface rendering shows a pore formed by the four helix bundle and closed by the steric block of the indole side chains. A probe radius of 1.4 Å was used to generate the surface.

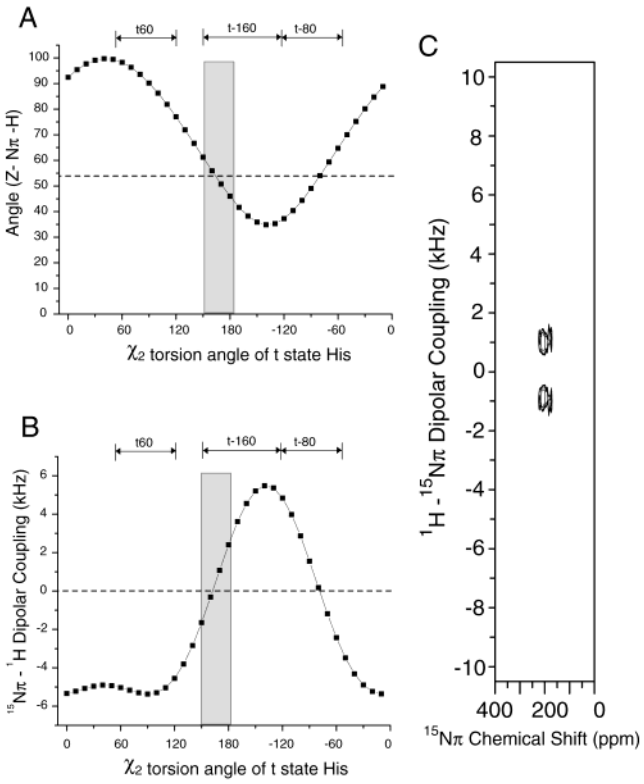

FIGURE 11: (A) Orientation of the N_π−H bond and (B) the prediction of the static $^{15}N_\pi$−^{1}H dipolar coupling for the observed histidine side chain torsion angle solution set. The angle is predicted to be near the magic angle with a resultant narrow range of dipolar couplings between −1.5 and +2.5 kHz. Note that the gray shadowed range is from the χ_2 rotamer angle search using the REDOR distance, which is now overlaid with the predicted dipolar coupling from PISEMA. (C) The PISEMA spectrum of $^{15}N_\pi$ labeled His37 M2-TMP. A dipolar coupling of 2 kHz is observed supporting the conformational analysis of this paper.

taking the motional averaged intra- and intermolecular dipolar interactions into account (data not shown). Consequently, it is concluded here that the dipolar dephasing is strictly due to a nearest neighbor intermolecular two spin system.

The left-handed sense for this helical bundle has been previously based on the tilt and rotational orientation of the helix combined with having the hydrophilic residues facing toward the pore instead of facing toward the lipid environment. Such positioning of the hydrophilic residues is based on mutagenesis studies and the favorable energetics of having the hydrophilic residues on the inside of the structure. A right-handed bundle would place the hydrophilic residues away from the pore to face the lipid environment. Here, it can be easily shown that the right-handed model is inconsistent with the short distance between His37 and Trp41. If these side chains face away from the pore of the tetrameric bundle, no possible combination of χ_1 and χ_2 angles would generate this close interresidue distance. Therefore, the left-handed helical sense of the bundle is now experimentally verified.

This model suggests that the orientation of the N_π−H bond relative to the magnetic field axis is close to the magic angle as shown in Figure 11A as a function of χ_2. Furthermore, the same region of χ_2 that is consistent with the common rotameric state of histidine and the observed distance to C_γTrp41 is highlighted. The range of N_π−H orientations predicted from the bundle structure is from 45° to 61°, corresponding to a dipolar coupling range of −1.5 to +2.5 kHz (Figure 11B). This dipolar coupling has been observed in a uniformly aligned sample using the PISEMA experiment (*24*). The observed coupling of 1.0 kHz (a dipolar splitting of 2 kHz; the sign is not defined using this experiment) is shown in Figure 11C, which is consistent with angles of 51° or 59° in the bundle structure.

It is unusual for a single distance measurement to be so effective in defining both the side chain conformations as well as significantly restraining the quarternary structure. The success of this effort lies in the short distance that was observed and the well-defined backbone structure and orientation of each helix with respect to the bilayer normal. The helical backbone is very well defined by the precise orientational restraints, which are absolute in that they relate each peptide plane relative to the fixed laboratory frame of reference. The resulting tetrameric structure is validated in a variety of ways. Both His and Trp side chains are oriented toward the pore, where they can play a significant functional role. The channel appears to be closed by the close proximity of the four indoles consistent with electrophysiology and mutagenesis studies of the intact protein at pH 7.0 and above. The pore maintains its integrity to the N terminal side of the membrane and at the same time a cavity is generated that appears adequate for binding amantadine. Finally, the observation of a 2 kHz coupling in the PISEMA spectrum of $^{15}N_\pi$His37 validates the structure based on the observed REDOR distance.

ACKNOWLEDGMENT

The authors thank Dr. Umesh Goli and Dr. Hank Henricks for their assistance with the peptide synthesis.

REFERENCES

1. Duff, K. C., and Ashley, R. H. (1992) *Virology 190*, 485−489.
2. Tosteson, M. T., Pinto, L. H., Holsinger, L. J., and Lamb, R. A. (1994) *J. Membr. Biol. 142*, 117−126.
3. Tang, Y., Zaitseva, F., Lamb, R. A., and Pinto, L. H. *J. Biol. Chem.*, in press.
4. Sakaguchi, T., Tu, Q., Pinto, L. H., and Lamb, R. A. (1997) *Proc. Natl. Acad. Sci. U.S.A. 94*, 5000−5005.
5. Lamb, R. A., Zebedee, S. L., and Richardson, C. D. (1985) *Cell 40*, 627−633.
6. Bron, R., Kendal, A. P., Klenk, H. D., and Wilschut, J. (1993) *Virology 195*, 808−811.
7. Lamb, R. A., Holsinger, L. J., and Pinto, L. H. (1994) in *Receptor-Mediated Virus Entry into Cell* (Wemmer, E., Ed.) Cold Spring Harbor Press, Cold Spring Harbor, New York.
8. Holsinger, L. J., and Lamb, R. A. (1991) *Virology 183*, 32−43.
9. Duff, K. C., Gilchrist, P. J., Saxena, A. M., and Bradshaw, J. P. (1994) *Virology 202*, 287−293.
10. Tobler, K., Kelly, M. L., Pinto, L. H., and Lamb, R. A. (1999) *J. Virology 73*, 9695−9701.
11. Kovacs, F. A., Denny, J. K., Song, Z., Quine, J. R., and Cross, T. A. (2000) *J. Mol. Biol. 295*, 117−125.
12. Salom, D., Hill, B. R., Lear, J. D., and DeGrado, W. F. (2000) *Biochemistry 39*, 14160−14170.
13. Wang, J., Kim, S., Kovacs, F., and Cross, T. A. (2001) *Protein Sci. 10*, 2241−2250.
14. Bauer, C. M., Pinto, L. H., Cross, T. A., and Lamb, R. A. (1999) *Virology 254*, 196−209.
15. Pinto, L. H., Dieckmann, G. R., Gandhi, C. S., Papworth, C. G., Braman, J., Shaughnessy, M. A., Lear, J. D., Lamb, R. A., and DeGrado, W. F. (1997) *Proc. Natl. Acad. Sci. U.S.A. 94*, 11301−11306.
16. Kovacs, F., and Cross, T. A. (1997) *Biophys. J. 73*, 2511−2117.

17. Sansom, M. S. P., Kerr, I. D., Smith, G. R., and Son, H. S. (1997) *Virology 233*, 163−173.
18. Zhong, Q., Husslein, T., Moore, P. B., Newns, D. M., Pattnaik, P., and Klein, M. L. (1998) *FEBS Lett. 434*, 265−271.
19. Kukol, A., Adams, P. D., Rice, L. M., Brunger, A. T., and Arkin, I. T. (1999) *J. Mol. Biol. 286*, 951−962.
20. Forrest, L. R., Kukol, A., Arkin, I. T., Tieleman, D. P., and Sansom, M. S. P. (1999) *Biophys. J. 78*, 55−69.
21. Schweighofer, K. J., and Pohorille, A. (2000) *Biophys. J. 78*, 150−163.
22. Fu, R., and Cross, T. A. (1999). *Annu. Rev. Biophys. Biomol. Struct. 28*, 235−268.
23. Cross, T. A., and Quine, J. R. (2000) *Concepts NMR 12*, 55−70.
24. Wu, C. H., Ramamoorthy, A., and Opella, S. J. (1994) *J. Magn. Reson.. Ser. A 109*, 270−272.
25. Wang, J., Denny, J., Tian, C., Kim, S., Mo, Y., Kovacs, F., Song, Z., Nishimura, K., Gan, Z., Fu, R., Quine, J., and Cross, T. A. (2000) *J. Magn. Reson. 144*, 162−167.
26. Marassi, F. M., and Opella, S. J. (2000) *J. Magn. Reson. 144*, 150−155.
27. Garbow, J. R., and McWherter, C. A. (1993) *J. Am. Chem. Soc. 115*, 238−244.
28. Naito, A., Nishimura, K., Kimura, S., Tuzi, S., Aida, M., Yasuoka, N., and Saito, H. (1996) *J. Phys. Chem. 100*, 14995−15004.
29. Nishimura, K., Naito, A., Hashimoto, C., Aida, M., Tuzi, S., and Saito, H. (1998) *J. Phys. Chem. B 102*, 7476−1783.
30. Nomura, K., Takegoshi, K., Terao, T., Uchida, K., and Kainosho, M. (2000) *J. Biomol. NMR 17*, 111−123.
31. Middleton, D. A., Robins, R., Feng, X., Levitt, M. H., Spiers, I. D., Schwlbe, C. H., Reid, D. G., and Watts, A. (1997) *FEBS Lett. 410*, 269−274.
32. Jakeman, D. L., Mitchell, D. J., Shuttleworth, W. A., and Evans, J. N. S. (1998) *Biochemistry 37*, 12012−12019.
33. Merritt, M. E., Sigurdsson, S. Th., and Drobny, G. P. (1999) *J. Am. Chem. Soc. 121*, 6070−6071.
34. Goetz, J. M., Poliks, B., Studelska, D. R., Fischer, M., Kugelbrey, K., Bacher, A., Cushman, M., and Schaefer, J. (1999) *J. Am. Chem. Soc. 121*, 7500−7508.
35. Balbach, J. J., Yang, J., Welicky, D. P., Steinbach, P. J., Tugarinov, V., Anglister, J., and Tycko, R. (2000) *J. Biomol. NMR 16*, 313−327.
36. Peerson, O. B., Yoshimura, S., Hojo, H., Aimoto, S., and Smith, S. O. (1992) *J. Am. Chem. Soc. 114*, 4332−4335.
37. Smith, S. O., and Borman, B. J. (1995) *Proc. Natl. Acad. Sci. 92*, 488−491.
38. Smith, S. O., Eilers, M., Song, M., Aimoto, S. (2002) *Biophys. J. 82*, 2476−2486.
39. Isaac, B., Gallagher, G. J., Balazs, Y. S., and Thompson, L. K. (2002) *Biochemistry 41*, 3025−3036.
40. Gullion, T., and Schaefer, J. (1989) *J. Magn. Reson. 81*, 196−200.
41. Fu, R., Cotten, M., and Cross, T. A. (2000) *J. Biomol. NMR 16*, 261−268.
42. Paquet, A. (1982) *Can. J. Chem. 60*, 976−980.
43. Barlos, K., Papaioannou, D., and Theodoropoulos, D. (1982) *J. Org. Chem.* 1324−1326.
44. Nishimura, K., Fu, R., and Cross, T. A. (2001) *J. Magn. Reson. 152*, 227−233.
45. Gullion, T., Baker, D., and Conradi, M. S. (1990) *J. Magn. Reson. 89*, 479−484.
46. Naito, A., Nishimura, K., Tuzi, S., and Saito, H. (1994) *Chem. Phys. Lett. 229*, 506−511.
47. Song, Z., Kovacs, F., Wang, J., Denny, J., Shekar, S. C., Quine, J., and Cross, T. A. (2000) *Biophys. J. 79*, 767−775.
48. Adams, P., Arkin, I., Engelman, D., and Brunger, A. T. (1995) *Nat. Struct. Biol. 2*, 154−162.
49. Torres, J., Kukol, A., and Arkin, I. (2001) *Biophys. J. 81*, 2681−2692.
50. Harris, N. L., Presnell, S. R., and Cohen, F. E. (1994) *J. Mol. Biol. 236*, 1356−1368.
51. Bywater, R. P., Thomas, D., and Vriend, G. (2001) *J. Comput. Aid. Mol. Des. 15*, 533−552.
52. Lovell, S. C., Word, J. M., Richardson, J. S., and Richardson, D. C. (2000) *Proteins 40*, 389−408.
53. Brooks, B. R., Bruccoleri, R. E., Olafson, B. D., States, D. J., Swaminathan, S., and Karplus, M. (1983) *J. Comput. Chem. 4*, 187−217.
54. Nishimura, K., Naito, A., Tuzi, S., and Saito, H. (1999) *J. Phys. Chem. B. 103*, 8398−8404.

BI0262799